Cooperative localization with angular measurements and posterior linearization

Cooperative Localization with Angular Measurements and Posterior Linearization

Yibo Wu*, Bile Peng*, Henk Wymeersch*, Gonzalo Seco-Granados‡,
Anastasios Kakkavas†§, Mario H. Castañeda Garcia†, and Richard A. Stirling-Gallacher†
*Department of Electrical Engineering, Chalmers University of Technology
†Munich Research Center, Huawei Technologies Duesseldorf GmbH
‡Department of Telecommunications and Systems Engineering, Universitat Autonoma de Barcelona
§Department of Electrical and Computer Engineering, Technische Universität München

***Abstract*—The application of cooperative localization in vehicular networks is attractive to improve accuracy and coverage of the positioning. Conventional distance measurements between vehicles are limited by the need for synchronization and provide no heading information of the vehicle. To address this, we present a cooperative localization algorithm using posterior linearization belief propagation (PLBP) utilizing angle-of-arrival (AoA)-only measurements. Simulation results show that both directional and positional root mean squared error (RMSE) of vehicles can be decreased significantly and converge to a low value in a few iterations. Furthermore, the influence of parameters for the vehicular network, such as vehicle density, communication radius, prior uncertainty, and AoA measurements noise, is analyzed.**

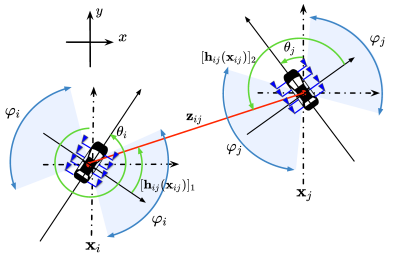

Fig. 1: Geometric model of two vehicles. Vehicle i measures the AoA $[\mathbf{h}_{ij}(\mathbf{x}_{ij})]_1$ from vehicle j, and vehicle j measures $[\mathbf{h}_{ij}(\mathbf{x}_{ij})]_2$.

I. Introduction

Vehicular localization with high precision is of great importance for future applications such as autonomous driving. Although the widely used localization technique global navigation satellite system (GNSS) can provide position information, it is limited by the poor signal penetration capabilities and has inadequate performance in some specific scenarios such as indoor environment. Cooperative localization [1] is a promising technique to improve the positioning accuracy and coverage. It enables vehicles to share orientation and position information to neighbours, and infer their own positions using these information. Generally, this inference process can be implemented by message passing (MP) algorithms such as Belief propagation (BP) [2]. In BP, messages are generated based on positioning information from on-board sensors, such as 5G front-end, radar, and stereo cameras [3], and then messages are propagated among vehicles' neighbours. Utilizing these BP messages, vehicles can update their local beliefs, i.e., vehicles update their own position and orientation states based on neighbours' information. Cooperative localization is particularly advantageous when vehicles have different prior localization accuracy, because vehicles with high-quality sensors can help vehicles with low quality sensors to reduce their localization errors. The last point is practical in the foreseeable future because vehicles with different levels of sensing precision are expected to coexist [4].

The performance of cooperative localization is limited by the underlying measurements. Conventional measurements include *distance* and *angle* between vehicles. In terms of distance measurements, radar can provide high accuracy, but does not include identity information of the target, which is required for MP algorithms. Measurements based on the travel time of radio signals (time-of-arrival (TOA) and time-difference-of-arrival (TDOA)) can provide such identity information [5]. However, TOA and TDOA are challenged by the synchronization requirements due to the clock difference between two vehicles, where even a small clock error can lead to significant localization error [6]. Alternatively, the two-way TOA can be used to avoid synchronization, but the delay time is doubled because of the round-trip characteristic which also increases the resource consumption. Besides, achieving a ranging accuracy lower than 10 m with TOA/TDOA is very challenging in vehicular environments [7]. In contrast, AoA is readily available when the receiver is equipped with an antenna array [8]–[11]: [10] has investigated the performance of vehicle-to-vehicle (V2V) relative positioning using AoA measurements from multiple receiving arrays on the vehicle, and the achieved positioning accuracy met requirements of 5G New Radio (NR) vehicle-to-everything (V2X) standardization.

While AoA measurements are attractive from a practical point of view, the integration with MP is non-trivial. Because the measurement function of the AoA measurement is non-linear, it is not possible to perform analytical computation of the messages in BP. One approach addressing this problem is to use non-parametric BP [12], which uses particles to approximates the BP messages. However, a large number of particles are required to achieve accurate performance, which increases the computation complexity dramatically. Another

solution is to perform linearization algorithm on the measurement model such as posterior linearization (PL) [13], so that the model can be integrated with parametric BP algorithms. For instance, Gaussian parametric BP can represent the BP messages as closed-form Gaussian distributions with the linearized observation model [14]. Reference [15] performs posterior linearization belief propagation (PLBP) in cooperative localization, and Gaussian parametric BP is integrated with the linearization algorithm PL, which performs statistical linear regression (SLR) on the distance measurement model. However, the scenario of using angular measurement model is not discussed, and only the position is considered as an unknown state. [11] considers a target tracking scenario, but angular measurements are represented by a von Mises-Fisher (VMF) distribution rather than Gaussian distribution, and only position errors are analyzed.

Extending the work in [15], we consider a cooperative localization problem where vehicles' positions and orientations are both unknown and only angular measurements can be observed. PLBP is also used to tackle the localization problem. The linearization algorithm PL linearizes the model with respect to the posterior state so that BP messages can be generated in Gaussian forms and then propagated among vehicles. Finally, these BP messages are used to update vehicle position and orientation states. This PLBP procedure is iterated until the posterior probability density function (PDF) of the vehicle position and orientation converge.

The paper is organized as follows. In Section II, we introduce the cooperative localization problem which includes the nonlinear angular measurement model and the localization algorithm. In Section III, we describe the implementation of PLBP on solving the localization problem. Section IV details the results of PLBP's performance on a realistic scenario in terms of both position and orientation accuracy. In Section V we draw our conclusion.

Notation: In this paper, the following notation will be used. The state of vehicle i will be denoted by $\mathbf{x}_i$ and the joint state of vehicle i and j will be denoted by $\mathbf{x}_{ij}$. Vectors will be written in bold and distributions such as $p_X(x)$ will be abbreviated by $p(x)$.

II. Problem Statement

We consider a network comprising a set of vehicles $\mathcal{V} = \{1, ..., N\}$ and a set of communication links $\mathcal{E} \subset \mathcal{V} \times \mathcal{V}$ to connect each vehicle according to a communication radius r. The neighbor set of vehicle i is denoted by $\mathcal{N}_i$. Each vehicle $i \in \mathcal{V}$ has a state $\mathbf{x}_i \in \mathbb{R}^3$, comprising the 2D position $[x_i, y_i]^\mathsf{T}$ and the heading $\theta_i \in (-\pi, \pi]$. We denote the joint state of vehicles i and j as $\mathbf{x}_{ij} = [\mathbf{x}_i^\mathsf{T} \mathbf{x}_j^\mathsf{T}]^\mathsf{T}$. Each vehicle is assumed to have knowledge of its prior state by some accessible positioning techniques, e.g., GNSS, assumed to be a Gaussian density

$$p_i(\mathbf{x}_i) = \mathcal{N}(\mathbf{x}_i; \boldsymbol{\mu}_i, \mathbf{P}_i), \tag{1}$$

where $\mathcal{N}(\mathbf{x}_i; \boldsymbol{\mu}_i, \mathbf{P}_i)$ denotes a Gaussian distribution in variable $\mathbf{x}_i$ with mean vector $\boldsymbol{\mu}_i = [\mu_x, \mu_y, \mu_\theta]^\mathsf{T}$ and covariance matrix $\mathbf{P}_i$. The measurement model between two vehicles is shown in Fig. 1. Each vehicle i is equipped with linear arrays on its two sides, each of which provides a field of view (FOV) φ_i with $0 < \varphi_i \leq \pi$. Signals with an AoA measurements within the FOV of node can be measured. The AoA measurement vector $\mathbf{z}_{ij}$ between vehicles i and j is defined as a function of $\mathbf{x}_i$ and $\mathbf{x}_j$ with additive Gaussian noise

$$\mathbf{z}_{ij} = \mathbf{h}_{ij}(\mathbf{x}_{ij}) + \boldsymbol{\eta}_{ij}, \tag{2}$$

where $\boldsymbol{\eta}_{ij}$ represents the measurement noise, modeled as $\boldsymbol{\eta}_{ij} \sim \mathcal{N}(\mathbf{0}, \mathbf{R}_{ij})$ and $\mathbf{h}_{ij}(\mathbf{x}_{ij})$ is defined as[1]

$$\mathbf{h}_{ij}(\mathbf{x}_{ij}) = \begin{bmatrix} \operatorname{atan2}\left((y_j - y_i), (x_j - x_i)\right) - \theta_i \\ \operatorname{atan2}((y_i - y_j), (x_i - x_j)) - \theta_j \end{bmatrix}, \tag{3}$$

in which $\operatorname{atan2}(y, x)$ calculate the four-quadrant inverse tangent of y and x. However, the $\operatorname{atan2}$ introduces problems because of its discontinuity at the negative semi-axis of x, i.e. $\operatorname{atan2}(x, 0) : x < 0$. Instead of modeling the angular measurements by VMF distribution, as [11] has done, we adopt an ad-hoc correction from [17] due to simplicity of implementation, which is described in Appendix A. We denote the vector of all measurements by $\mathbf{z} = [\mathbf{z}_{ij}]_{i,j \in \mathcal{N}_i}$ and the vector of all vehicles' states by $\mathbf{x}$.

Our goal is to compute the marginal distribution $p_i(\mathbf{x}_i|\mathbf{z})$ for each vehicle in this network, i.e., calculate the posterior state of each vehicle with received nearby information and angular measurements. To achieve this cooperative positioning goal, we consider the combination of low-complexity Gaussian BP with a linearization algorithm to approximate the nonlinear angular measurement model.

III. Belief Propagation and Posterior Linearization

In this section we describe how the algorithm PLBP solves the cooperative localization problem. In PLBP, BP is selected as the MP algorithm, which is described in Section III-A. To calculate the BP messages in Gaussian form, the linearization algorithm PL linearizes the angular measurement model, which is illustrated in Section III-B. Finally, PLBP integrates the BP and PL together in an iterative way, presented in Section III-C.

A. Belief Propagation Formulation

The joint PDF of a factor graph can be factorized into

$$p(\mathbf{x}, \mathbf{z}) = p(\mathbf{x}) p(\mathbf{z}|\mathbf{x}) \tag{4}$$

$$= \prod_{i=1}^{N} p_i(\mathbf{x}_i) \prod_{j \in \mathcal{N}_i, j > i} p(\mathbf{z}_{ij}|\mathbf{x}_{ij}), \tag{5}$$

[1]For simplicity we consider the center points of the two arrays on each vehicle to coincide. The effect of the relative position and orientation of the antenna arrays is outside the scope of this paper and related work can be found in [16].

and BP can be performed on this graph to compute approximations of the marginal posteriors $p_i(\mathbf{x}_i|\mathbf{z})$. The BP message passing rules at iteration k are as follows (assuming $j \in \mathcal{N}_i$) [2]

$$b_j^{(k-1)}(\mathbf{x}_j) \propto p_j(\mathbf{x}_j) \prod_{i \in \mathcal{N}_j} m_{i\to j}^{(k-1)}(\mathbf{x}_j) \tag{6}$$

$$m_{j\to i}^{(k)}(\mathbf{x}_i) \propto \int p(\mathbf{z}_{ij}|\mathbf{x}_{ij}) \frac{b_j^{(k-1)}(\mathbf{x}_j)}{m_{i\to j}^{(k-1)}(\mathbf{x}_j)} \mathrm{d}\mathbf{x}_j \tag{7}$$

where $b_j^{(k-1)}(\mathbf{x}_j)$ denotes the local belief of $\mathbf{x}_j$ at iteration $k-1$, and $m_{j\to i}^{(k)}(\mathbf{x}_i)$ denotes the BP message from $\mathbf{x}_j$ to $\mathbf{x}_i$ at iteration k. The BP process is initialized at $k=0$ by $b_j^{(0)}(\mathbf{x}_j) = p_j(\mathbf{x}_j)$ and $m_{i\to j}^{(0)}(\mathbf{x}_j) = 1$. The approximate marginal posterior of $\mathbf{x}_j$ at iteration k is $p_j(\mathbf{x}_j|\mathbf{z}) \approx b_j^{(k)}(\mathbf{x}_j)$. Similarly, the joint posterior of $\mathbf{x}_i, \mathbf{x}_j$ can also be approximated by [2]

$$b^{(k)}(\mathbf{x}_{ij}) \propto p(\mathbf{z}_{ij}|\mathbf{x}_{ij}) \frac{b_i^{(k)}(\mathbf{x}_i) b_j^{(k)}(\mathbf{x}_j)}{m_{i\to j}^{(k)}(\mathbf{x}_j) m_{j\to i}^{(k)}(\mathbf{x}_i)}. \tag{8}$$

However, due to the nonlinear observation model (2), in general BP cannot be executed in closed form: neither the integral (6) nor the product (7) can be computed exactly, except when the observation model is linear with Gaussian noise [13]. This motivates the following linearization procedure.

B. Posterior Linearization

The observation model can be linearized as

$$\mathbf{h}_{ij}(\mathbf{x}_{ij}) \approx \mathbf{C}_{ij}\tilde{\mathbf{x}}_{ij} + \mathbf{e}_{ij}, \tag{9}$$

where $\mathbf{e}_{ij} \sim \mathcal{N}(\mathbf{0}, \mathbf{\Omega}_{i,j})$, and $\tilde{\mathbf{x}}_{ij} = [\mathbf{x}_{ij}^\mathsf{T}\ \mathbf{1}^\mathsf{T}]^\mathsf{T}$. The target is to find $\mathbf{C}_{ij}$ that minimizes the mean square error (MSE) between the measurement function $\mathbf{h}_{ij}(\mathbf{x}_{ij})$ and the approximated function:

$$\arg\min_{\mathbf{C}_{ij}} \mathbb{E}\{\|\mathbf{h}_{ij}(\mathbf{x}_{ij}) - \mathbf{C}_{ij}\tilde{\mathbf{x}}_{ij}\|^2\}, \tag{10}$$

and we can calculate the MSE error $\mathbf{\Omega}_{i,j} = \|\mathbf{h}_{ij}(\mathbf{x}_{ij}) - \mathbf{C}_{ij}\tilde{\mathbf{x}}_{ij}\|^2$. To solve this optimization problem, PL [13] is performed, which solves $\mathbf{C}_{ij}$ by SLR [13] with respect to the posterior PDF, and details are presented in Appendix A. Fig. 2 provides an example to visualize the advantage of posterior linearization. We observe that the model linearized by posterior is closer to the true model than the model linearized by prior because the posterior distribution are more accurate to the true state, and the former linearized model is shorter than the latter linearized model because of less uncertainty in posterior PDF.

C. Belief Propagation with Linearized Measurement Models

Once all measurement models are approximated, BP can be performed in Gaussian format. The likelihood function is of the form

$$p(\mathbf{z}_{ij}|\mathbf{x}_{ij}) \propto \exp\left(-\frac{1}{2}(\mathbf{z}_{ij} - \mathbf{C}_{ij}\tilde{\mathbf{x}}_{ij})^\mathsf{T} \mathbf{\Sigma}_{ij}^{-1} (\mathbf{z}_{ij} - \mathbf{C}_{ij}\tilde{\mathbf{x}}_{ij})\right), \tag{11}$$

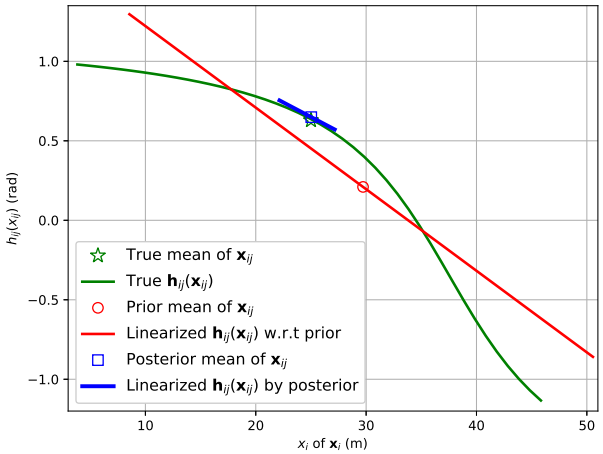

Fig. 2: An example of the true measurement model $\mathbf{h}_{ij}(\mathbf{x}_{ij})$ and its approximations with respect to prior and posterior, as a function of the x-position of $\mathbf{x}_i$. Compared to linearized model from the prior, the model linearized from the posterior is more accurate and has less uncertainty (shorter length).

where $\mathbf{\Sigma}_{ij} = \mathbf{\Omega}_{ij} + \mathbf{R}_{ij}$. This formulation allows closed-form Gaussian messages passing using (6)–(7) and (8), and details of this implementation are provided in the Appendix B.

The overall algorithm thus operates as described in Algorithm 1. The algorithm requires a selection of K (the number of linearization iterations) and M (the number of BP iterations per linearization step). The overall complexity per vehicle is approximately $\mathcal{O}(KM\bar{N}D^3)$, where D is the state dimension and $\bar{N}$ is the average number of neighbors.

Algorithm 1 : Iterative Cooperative Localization

for $k = 1$ to K **do**
  Given the current beliefs $b^{(k-1)}(\mathbf{x}_{ij})$, solve (10) for each $(i,j) \in \mathcal{E}$ to obtain (11).
  Run M iterations of BP on the linearized model.
  Compute joint beliefs $b^{(k)}(\mathbf{x}_{ij})$ at the current BP iteration.
end for
Return marginal beliefs.

IV. Simulation Results

In this section we simulated a vehicular network scenario which is close to the situation in real life, and the performance of Algorithm 1 is evaluated by the root mean squared error (RMSE) in position and orientation. Then, based on this scenario, we analyzed the impact of different network parameters on the performance.

A. Simulation Scenario

The vehicular scenario is based on a road map in central New York Manhattan (latitude: 40.71590 and longitude: -73.99560). The map data is generated from Stamen Map [18] at a zoom level of 18. Within this map, the scenario is shown in Fig. 3, where 51 vehicles are possibly connected within the communication radius ($r = 30$ m). The priors are set to

TABLE I: Setup parameters for the vehicular scenario.

r [m]	φ [rad]	σ_x [m]	σ_y [m]	σ_θ [rad]	R [rad^2]
30	π	5	5	0.35	0.10

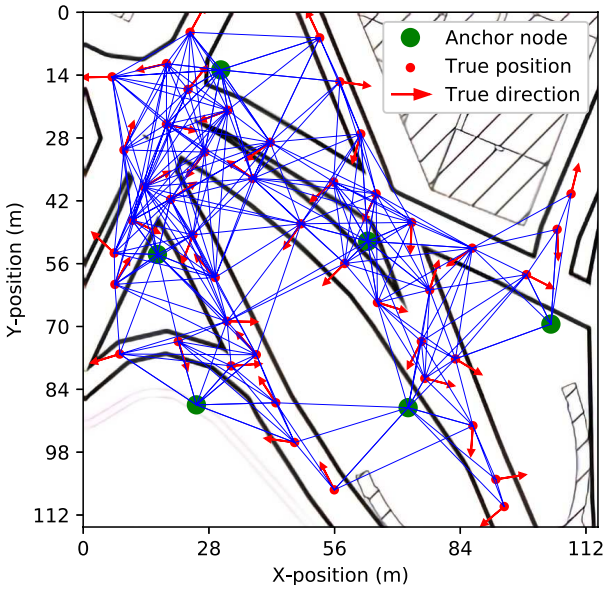

Fig. 3: Scenario of the vehicular network before applying PLBP, and average position and orientation RMSEs are 7.01m and 0.38 rad, respectively. The interactive web map can be found at [20]. The convergence situation after applying PLBP can be found at [19] with decreased average RMSEs, 1.49m and 0.044 rad.

$\mathbf{P}_i = \text{diag}(\sigma_x^2, \sigma_y^2, \sigma_\theta^2)$. Among the vehicles, 6 are chosen as anchors (vehicles or road side units with a very concentrated prior density, set to $\text{diag}(\sigma_x^2, \sigma_y^2, \sigma_\theta^2) = \text{diag}(0.01, 0.01, 0.01)$), and the selection of anchors is out of the scope of this paper. The interactive web map is also provided[2] in [20]. The remaining parameters of this scenario are illustrated in Table I, where R denotes the constant value of the measurement variance (approximately 18 degrees standard deviation).

B. Results and Discussion

1) Convergence Speed: In order to examine the performance of Algorithm 1, in Fig. 4 we plot the RMS position and direction error against the number of linearization iteration K. Notice the performance gap between the prior linearization filter (LF) (dotted lines) and the posterior LF (solid lines). After each belief propagation iteration, the posterior of each vehicle is closer to the true state than the prior, so the belief propagation has a better performance on the posterior linearization measurement model. Both position RMSE and direction RMSE converged for linearization iteration number larger than 4. Meanwhile, increasing M from 1 to 3 provides significant improvements for both position and orientation estimation accuracy as the beliefs are more accurate. The improvement becomes very small for M greater than 3.

[2]The convergence situation of Fig. 3 can be visualized by an interactive web map in [19], where the red, blue, and green dots represent the true, prior and estimated positions, respectively.

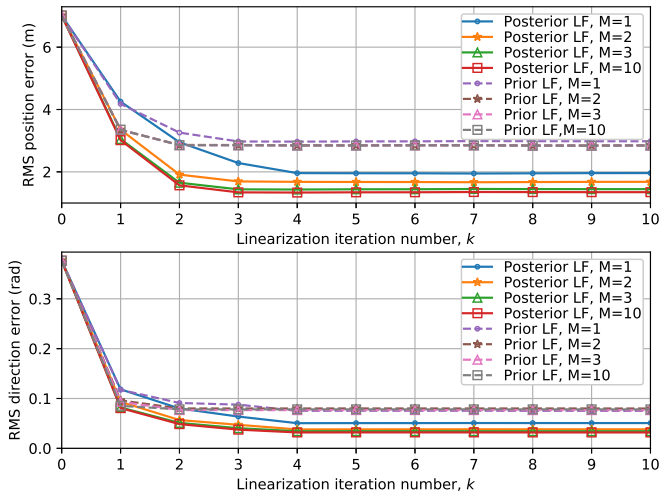

Fig. 4: RMS position and direction error against the number of linearization iteration k. The initial position and direction RMSE of vehicles are 7.01m and 0.38 rad, respectively.

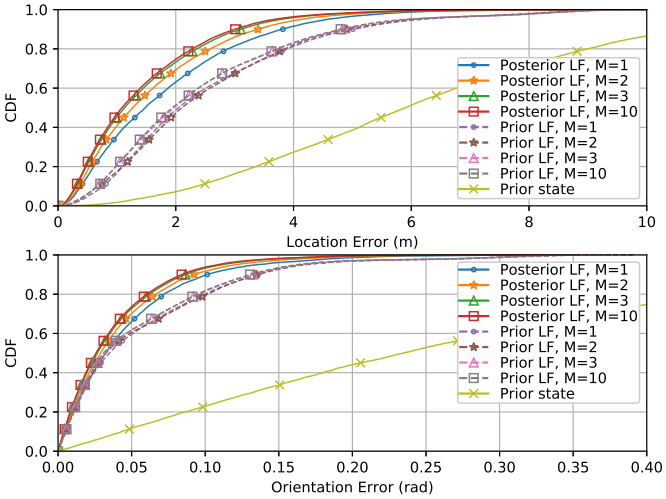

Fig. 5: CDF of location and orientation errors, $K = 10$.

2) Localization Performance: While the above results show the average RMSE of the position and direction, Fig. 5 shows the cumulative distribution functions (CDFs) of the position and direction errors for $K = 10$ for different values of M. We observe that for $M = 3$ the performance is similar to $M = 10$ and that nearly all vehicles can be localized with a position error less then 4 meters and an orientation error less than 0.15 radians (8 degrees). The advantageous performance of posterior linearization BP over prior linearization BP is clear.

3) Impact of Network parameters: Here, we analyze the impact of modifying the scenario parameters in Table I on localization and orientation estimation performance. In Fig. 6, we evaluate 4 parameters separately, namely communication radius (r), measurement noise variance (R), prior uncertainty in position ($\sigma_p = (\sigma_x^2 + \sigma_y^2)^{1/2}$) and prior uncertainty in orientation (σ_θ) in 4 sub-figures, by plotting the position and direction RMSE as functions of one of them, while keeping

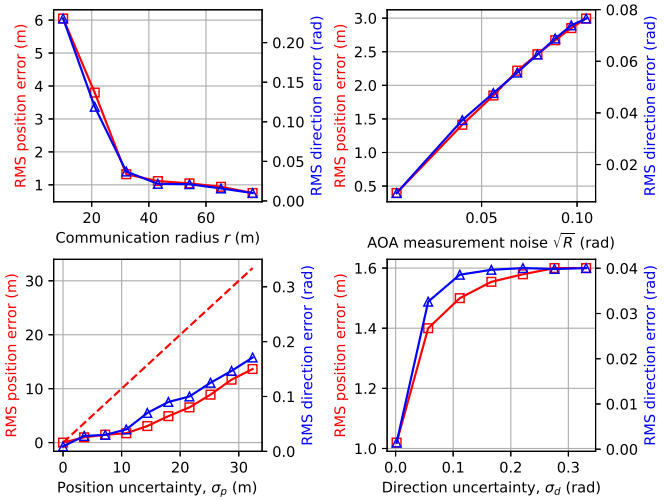

Fig. 6: The impact of 4 vehicle network parameters on localization and orientation performance. Lines with square and triangle markers represent the position and orientation RMSE, respectively. $K = 10$, $M = 10$ and posterior LF are applied.

the rest fixed to the values of Table I.

- The top left sub-figure shows the impact of the communication radius r. Both RMSEs are reduced rapidly by increasing r from 10 m to 30 m since each vehicle has more neighbors and the network connectivity increases quickly, up to the point where all vehicles are in each others' communication range. We note that with increased connectivity comes increased computational complexity.
- In the top right sub-figure, we vary the AoA measurements noise variance R. We note that both direction and position RMSE increase approximately linearly in $\sqrt{R}$. This emphasizes the need for good measurements.
- The influence of the prior position uncertainty ($\sqrt{\sigma_x, \sigma_y}$) is shown in the bottom left sub-figure. The red dashed line describes the prior position RMSE. We notice the increase of σ_p from 0 m to 10 m has small effect on both position and direction performance (less than 2 m/0.05 rad), showing the good performance of the proposed method. For position uncertainty over 10 m, Algorithm 1 is still able to improve performance over the prior RMSE, but leads to progressively larger errors. This is in contrast to range-based cooperative localization [1], where no prior information was needed.
- The influence of the direction uncertainty (σ_θ) is shown in the bottom right sub-figure, where we observe a rapid increase in RMSE. This is because the AoA measurements depend on the orientation of the receiving vehicles. For larger prior orientation uncertainty, Algorithm 1 is less affected.

V. Conclusion

We have applied PLBP to cooperative localization (position and orientation estimation) of vehicles with AoA-only measurements. Numerical results show that PLBP can perform cooperative localization on vehicle networks with angular observation model and AoA measurements, and has good estimation performance in both position and orientation. Only a few iterations are required for convergence, which makes the algorithm attractive for real-time processing. Besides, the impact of multiple network conditions, including communication radius, position and orientation uncertainties, and measurement noise variance, has been analyzed. A comparison to non-parametric BP is left for future work.

Acknowledgment

This research was supported, in part, by the EU Horizon 2020 project 5GCAR (Fifth Generation Communication Automotive Research and innovation) and the Spanish Ministry of Science, Innovation and Universities under Grant TEC2017-89925-R.

Appendix A
Steps of the Posterior Linearization

This section illustrates the procedures of SLR on the measurement model and the approximation of the parameters $(\mathbf{C}_{ij}, \mathbf{\Omega}_{i,j})$ with respect to the joint posterior PDF $p(\mathbf{x}_{ij}|\mathbf{z}_{ij}) = \mathcal{N}(\mathbf{x}_{ij}; \boldsymbol{\mu}_{ij}; \mathbf{P}_{ij})$. First, according to the joint posterior of $\mathbf{x}_i, \mathbf{x}_j$, we select L sigma-points $\mathcal{X}_1, ..., \mathcal{X}_L$ and weights $\omega_1, ..., \omega_L$ using a sigma-point method such as the unscented transform [21]. Then we calculate the transformed sigma points by

$$\mathcal{Z}_l = \mathbf{h}_{ij}(\mathcal{X}_l) \quad l = 1, ..., L \tag{12}$$

However, as mentioned in Section II, the function arctan has discontinuity problem at the negative x semi-axis. The sigma points transformation needs an ad-hoc modification so that the difference between angles $\mathcal{Z}_l - \mathbf{z}_{ij}$ must be bounded in $\pm\pi$. $\mathcal{Z}_l$ can be corrected to $\hat{\mathcal{Z}}_l$ by the following transformation:

$$\hat{\mathcal{Z}}_l = \mathbf{z}_{ij} + \pi - \text{modulo}((\mathbf{z}_{ij} - \mathcal{Z}_l) + \pi)_{2\pi} \tag{13}$$

where $\hat{\mathcal{Z}}_l$ denotes the corrected sigma point, z_{ij} is the AoA measurements and modulo$(\cdot)_{2\pi}$ represents the modulo operation.

Introducing $\mathbf{C}_{ij} = [\mathbf{A}_{ij} \ \mathbf{b}_{ij}]$, so that

$$\mathbf{h}_{ij}(\mathbf{x}_{ij}) \approx \mathbf{A}_{ij}\mathbf{x}_{ij} + \mathbf{b}_{ij} + \mathbf{e}_{ij}, \tag{14}$$

the solution of the approximation of $\mathbf{A}_{ij}, \mathbf{b}_{ij}, \Omega_{i,j}$ is

$$\mathbf{A}_{ij} = \mathbf{C}_{xz}^{\mathsf{T}}\mathbf{P}_{ij}^{-1} \tag{15}$$

$$\mathbf{b}_{ij} = \bar{z} - \mathbf{A}_{ij}\boldsymbol{\mu}_{ij} \tag{16}$$

$$\mathbf{\Omega}_{i,j} = \mathbf{C}_{zz} - \mathbf{A}_{ij}\mathbf{P}_{ij}\mathbf{A}_{ij}^{\mathsf{T}} \tag{17}$$

where $\bar{z}$, $\mathbf{C}_{xz}$ and $\mathbf{C}_{zz}$ are approximated using the sigma-points (13) and weights by

$$\bar{z} \approx \sum_{j=1}^{L} \omega_j \hat{\mathcal{Z}}_l \tag{18}$$

$$\mathbf{C}_{xz} \approx \sum_{j=1}^{L} \omega_j (\mathcal{X}_j - \boldsymbol{\mu}_{ij})(\hat{\mathcal{Z}}_l - \bar{z})^{\mathsf{T}} \tag{19}$$

$$\mathbf{C}_{zz} \approx \sum_{j=1}^{L} \omega_j (\hat{\mathcal{Z}}_l - \bar{z})(\hat{\mathcal{Z}}_l - \bar{z})^{\mathsf{T}}. \tag{20}$$

APPENDIX B
IMPLEMENTATION OF BP IN THE LINEARIZED MODEL

This section illustrates the derivation of equation (6)–(7) and (8). Once we have the approximated linearization model 9, we can represent the BP message $m_{i\to j}^{(k)}$ by the Gaussian format [15]

$$m_{i\to j}^{(k)}(\mathbf{x}_j) \propto \mathcal{N}(\boldsymbol{\alpha}_{ij}^{(k)}; \mathbf{H}_{ij}^{(k)}\mathbf{x}_j, \boldsymbol{\Gamma}_{ij}^{(k)}) \tag{21}$$

where $\boldsymbol{\alpha}_{ij}^{(k)}$, $\mathbf{H}_{ij}^{(k)}$ and $\boldsymbol{\Gamma}_{ij}^{(k)}$ are

$$\boldsymbol{\alpha}_{ij}^{(k)} = [\mathbf{z}_{ij}]_1 - \mathbf{A}_i \boldsymbol{\mu}_{ij}^{(k-1)} - b_{ij} \tag{22a}$$

$$\mathbf{H}_{ij}^{(k)} = \mathbf{A}_j \tag{22b}$$

$$\boldsymbol{\Gamma}_{ij}^{(k)} = \mathbf{R}_{ij} + \boldsymbol{\Omega}_{ij} + \mathbf{A}_i \mathbf{P}_{ij}^{(k-1)} \mathbf{A}_i^{\mathsf{T}} \tag{22c}$$

where $[\mathbf{z}_{ij}]_1$ is the AoA measurement received by vehicle i, $\mathbf{A}_i, \mathbf{A}_j$ are defined at Section III-B and $\boldsymbol{\mu}_{ij}^{(k-1)}$ and $\mathbf{P}_{ij}^{(k-1)}$ are found from the relation

$$\mathcal{N}(\boldsymbol{\mu}_{ij}^{(k-1)}, \mathbf{P}_{ij}^{(k-1)}) \propto \mathcal{N}(\mathbf{x}_i; \boldsymbol{\mu}_i, \mathbf{P}_i) \prod_{j' \in \mathcal{N}_i \setminus j} m_{j'\to i}^{(k-1)}(\mathbf{x}_i) \tag{23}$$

where the Kalman update step [15, Algorithm 1] is performed to update each message $m_{j'\to i}^{(k-1)}(\mathbf{x}_i)$ on the prior state $\mathcal{N}(\mathbf{x}_i; \boldsymbol{\mu}_i, \mathbf{P}_i)$.

To get the local belief (6) at the k-th iteration, we can also use Kalman filter update step to update the vehicle prior with all its incoming messages.

$$b_j^{(k)}(\mathbf{x}_j) = \mathcal{N}(\mathbf{x}_j; \boldsymbol{\mu}_j, \mathbf{P}_j) \times \prod_{i \in \mathcal{N}_j} m_{i\to j}^{(k)}(\mathbf{x}_j) \tag{24}$$

The k-th iteration joint posterior (8) is expressed as [15]

$$b^{(k)}(\mathbf{x}_{ij}) = \mathcal{N}(\mathbf{x}_i; \boldsymbol{\mu}_i, \mathbf{P}_i) \prod_{j' \in \mathcal{N}_i \setminus j} m_{j'\to i}^{(k)}(\mathbf{x}_i) \tag{25}$$
$$\times \mathcal{N}(\mathbf{x}_j, \boldsymbol{\mu}_j, \mathbf{P}_j) \times \prod_{i' \in \mathcal{N}_j \setminus i} m_{i'\to j}^{(k)}(\mathbf{x}_j) p(\mathbf{z}_{ij} | \mathbf{x}_i, \mathbf{x}_j)$$

where we can also apply Kalman filter update [15, Algorithm 1] as in (23).

REFERENCES

[1] H. Wymeersch, J. Lien, and M. Z. Win, "Cooperative localization in wireless networks," *Proc. IEEE*, vol. 97, no. 2, pp. 427–450, Feb 2009.

[2] F. R. Kschischang, B. J. Frey, H.-A. Loeliger *et al.*, "Factor graphs and the sum-product algorithm," *IEEE Trans. Inf. Theory.*, vol. 47, no. 2, pp. 498–519, Jul. 2001.

[3] F. de Ponte Müller, "Survey on ranging sensors and cooperative techniques for relative positioning of vehicles," *Sensors*, vol. 17, no. 2, p. 271, Jan. 2017.

[4] E. Steinmetz, R. Emardson, F. Brännström, and H. Wymeersch, "Theoretical limits on cooperative positioning in mixed traffic," *IEEE Access*, vol. 7, pp. 49 712–49 725, 2019.

[5] M. R. Gholami, S. Gezici, E. G. Strom, and M. Rydstrom, "Hybrid TW-TOA/TDOA positioning algorithms for cooperative wireless networks," in *IEEE Int. Conf. Commun.*, Jul. 2011, pp. 1–5.

[6] R. M. Buehrer, H. Wymeersch, and R. M. Vaghefi, "Collaborative sensor network localization: Algorithms and practical issues," *Proc. IEEE*, vol. 106, no. 6, pp. 1089–1114, Jun. 2018.

[7] N. Alam and A. G. Dempster, "Cooperative positioning for vehicular networks: Facts and future," *IEEE Trans. Intell. Transp. Syst.*, vol. 14, no. 4, pp. 1708–1717, Jun. 2013.

[8] S. Sakagami, S. Aoyama, K. Kuboi, S. Shirota, and A. Akeyama, "Vehicle position estimates by multibeam antennas in multipath environments," *IEEE Trans. Veh. Technol.*, vol. 41, no. 1, pp. 63–68, Feb. 1992.

[9] A. Fascista, G. Ciccarese, A. Coluccia, and G. Ricci, "Angle of arrival-based cooperative positioning for smart vehicles," *IEEE Trans. Intell. Transp. Syst.*, no. 99, pp. 1–13, Nov. 2017.

[10] A. Kakkavas, M. H. C. Garcia, R. A. Stirling-Gallacher, and J. A. Nossek, "Multi-array 5G V2V relative positioning: Performance bounds," in *IEEE Global Commun. Conf.*, Dec. 2018, pp. 206–212.

[11] A. F. Garcia-Fernandez, F. Tronarp, and S. Sarkka, "Gaussian target tracking with direction-of-arrival von Mises-Fisher measurements," *IEEE Trans. Signal Process.*, Apr. 2019.

[12] B. Etzlinger, F. Meyer, A. Springer, F. Hlawatsch, and H. Wymeersch, "Cooperative simultaneous localization and synchronization: A distributed hybrid message passing algorithm," in *Asilomar Conf. Signals, Systems and Computers.*, Nov. 2013, pp. 1978–1982.

[13] Á. F. García-Fernández, L. Svensson, M. R. Morelande, and S. Särkkä, "Posterior linearization filter: Principles and implementation using sigma points," *IEEE Trans. Signal Process.*, vol. 63, no. 20, pp. 5561–5573, Jul. 2015.

[14] W. Yuan, N. Wu, B. Etzlinger, H. Wang, and J. Kuang, "Cooperative joint localization and clock synchronization based on Gaussian message passing in asynchronous wireless networks." *IEEE Trans. Veh. Technol.*, vol. 65, no. 9, pp. 7258–7273, Jan. 2016.

[15] Á. F. García-Fernández, L. Svensson, and S. Särkkä, "Cooperative localization using posterior linearization belief propagation," *IEEE Trans. Veh. Technol.*, vol. 67, no. 1, pp. 832–836, Jan. 2018.

[16] Y. Shen and M. Z. Win, "On the accuracy of localization systems using wideband antenna arrays," *IEEE Trans. Commun.*, vol. 58, no. 1, pp. 270–280, Jan. 2010.

[17] D. F. Crouse, "Cubature/unscented/sigma point Kalman filtering with angular measurement models," in *18th Int. Conf. Inf. Fusion.*, Jul. 2015, pp. 1550–1557.

[18] Stamen-Map, "Map of central Manhattan," 2019, [Online]. Available: http://maps.stamen.com/m2i/#toner/256:256/18/40.71590/-73.99560.

[19] Y. Wu, "Convergence map of the vehicular network scenario," 2019, [Online]. Available: https://hhsly.github.io/paper-plbp-fig3/.

[20] ——, "Initialization map of the vehicular network scenario," 2019, [Online]. Available: https://hhsly.github.io/paper-plbp-fig3/.

[21] S. J. Julier and J. K. Uhlmann, "Unscented filtering and nonlinear estimation," *Proc. IEEE*, vol. 92, no. 3, pp. 401–422, 2004.